Hindawi
Mathematical Problems in Engineering
Volume 2022, Article ID 3154854, 11 pages
https://doi.org/10.1155/2022/3154854

Research Article

Aircraft Target Classification Method for Conventional Narrowband Radar Based on Micro-Doppler Effect

Saiqiang Xia,[1] **Chaowei Zhang**,[1] **Wanyong Cai**,[1] **Jun Yang**,[1] **Liangfa Hua**,[1] **Xu Wei**,[1] **and Haiman Jiang**[2]

[1]*Air Force Early Warning Academy, Wuhan 430019, China*
[2]*National University of Defense Technology, Nanjing 210012, China*

Correspondence should be addressed to Saiqiang Xia; xiasaiqiang@163.com

Received 16 November 2021; Revised 18 December 2021; Accepted 20 December 2021; Published 4 January 2022

Academic Editor: Fangqing Wen

For a conventional narrowband radar system, its insufficient bandwidth usually leads to the lack of detectable information of the target, and it is difficult for the radar to classify the target types, such as rotor helicopter, propeller aircraft, and jet aircraft. To address the classification problem of three different types of aircraft target, a joint multifeature classification method based on the micro-Doppler effect in the echo caused by the target micromotion is proposed in this paper. Through the characteristics analysis of the target simulation echoes obtained from the target scattering point model, four features with obvious distinguishability are extracted from the time domain and frequency domain, respectively, that is, flicker interval, fractal dimension, modulation bandwidth, and second central moment. Then, a support vector machine model will be applied to the classification of the three different types of aircraft. Compared with the conventional method, the proposed method has better classification performance and can significantly improve the classification probability of aircraft target. The simulations are carried out to validate the effectiveness of the proposed method.

1. Introduction

Modern warfare is a four-dimensional integration of land, sea, air, and space, in which the aircraft target has the superiority of high mobility and usually acts as the vanguard of the war. Generally speaking, there are three types of aircraft on the battlefield: rotor helicopter, propeller aircraft, and jet aircraft. It is necessary for the defense side to classify and identify the target of air intrusion in time to respond to the potential menaces and formulate their corresponding response strategies. In 2014, the Malaysia Airlines MH17 was shot down in eastern Ukraine due to the poor classification and identification ability of aircraft target, which caused a huge humanitarian crisis and reflected the necessity of the research on aircraft target classification and identification.

Since the range resolution of conventional narrowband radar is larger than the physical size of the target, less effective information can be extracted from the radar echo. Also, its mechanical scanning mode may lead to short target observation time, which makes it difficult to classify and identify the target under the low-resolution radar system. Compared with the working mode of using low-resolution radar to search targets with high-resolution radar for target classification, if the function of target classification can be directly extended in low-resolution radar, it can not only avoid the system complexity brought by large bandwidth to the radar but also greatly optimize the operational performance of the existing narrowband radar. It provides favorable support for the improvement of radar back-end informatization and decision-making strike in the combat process.

In the field of aircraft target classification and identification, the research on broadband radar is widely reported, and most of its main methods are based on high-resolution range profile [1–3], inverse synthetic aperture imaging [4, 5], and image processing [6–8]. New regime radars, such as MIMO radar [9–11], have achieved high precision target tracking and superresolution estimation of parameters, and

many useful explorations have already been conducted in the field of target identification. For conventional narrowband radar, most researchers multiple echo features and use support vector machine (SVM) classifiers to classify aircraft target types [12–20]. For example, [17] focuses on the difference of three types of aircraft target echoes in the Doppler domain, decomposes the echo by using empirical mode decomposition (EMD) algorithm, and then regards the waveform entropy, energy ratio, and second central moment of the decomposed intrinsic mode function (IMF) as a feature combination. Finally, the target classification is successfully achieved through the SVM classifier. However, this method not only is computationally intensive but also requires a high signal-to-noise ratio (SNR), and the classification performance degrades rapidly once the signal is contaminated by noise. Reference [18] extracts features with obvious differentiation such as Doppler shift, relative amplitude and waveform entropy in time and frequency domains, and Rayleigh entropy of time-frequency spectrum through feature analysis of a large amount of measured echo data. However, this method has obvious drawbacks: (1) using the Doppler shift as a classification feature must ensure that the flight directions of three types of targets do not differ greatly, which is basically impossible for the noncooperative target. (2) The combination of features is susceptible to other factors, and the robustness is poor. (3) The acquisition of feature values in the time-frequency domain must use the time-frequency analysis, which has a large amount of operations and cannot meet the real-time requirements of radar work. Reference [19] realizes aircraft target classification by extracting fractal and amplitude fluctuation. The advantage of this method is that it achieves a high classification probability with fewer feature values, and its drawback is that although the amplitude fluctuation can characterize the undulation characteristic of the echo, the feature is susceptible to noise interference and not robust under low SNR condition. In [20], the scattering point model is used to model three types of target. The sparse echo data is obtained by simulation, the echo is reconstructed by orthogonal matching pursuit algorithm (OMP) and smooth L0 norm reconstruction algorithm, and the amplitude fluctuation and waveform entropy are extracted. The shortcoming of this method is that the proposed target model is only equivalent by a small number of scattering points, and the model is too simple and does not consider the effects of fuselage and flight attitude, which is inconsistent with the actual situation.

To address the shortcomings of existing methods, this paper proposes a set of robust feature combinations based on the micro-Doppler effect, which can make full use of the information of the echo fuselage component and the micromotion component with a small amount of computation and strong noise immunity. Firstly, the radar echoes are generated by scattering point model simulation, pulse compression is conducted, and clutter suppression is performed by using adaptive complex variational modal decomposition. Then, the flicker interval and fractal dimension are extracted in time domain, modulation bandwidth and second central moment are extracted in frequency domain as a feature combination, and three binary SVM classifier is used for classification. Simulation results show that the proposed method has faster classification speed and better classification performance than the existing methods.

2. Echo Model

The radar echo of an aircraft target is the vector sum of the fuselage echo and the rotating parts echo, and the fuselage part has only translational components, while in addition to the translational components, the rotating parts still have some micromotion components; thus, this paper mainly gives the radar echo model of the rotating parts. Taking the helicopter as an example, the position relationship between the target and the radar is shown in Figure 1. The radar coordinate system $O-UVW$ is established with the radar position O as its origin, and the reference coordinate system $Q-XYZ$ is established with the center of the helicopter rotor Q as its origin, where the XY plane remains horizontal and the X axis is parallel to the U axis. At the same time, the target coordinate system $Q-xyz$ is established where the rotor is located as the surface xy. Let the distance from the radar to the target be R_0 and its pitch angle and azimuth angle be α and β, respectively, where $0 \le \alpha \le \pi/2$. For the convenience of analysis and without loss of generality, this paper assumes that the radar beam illuminates the target at $\beta = 0$.

Let the radar transmit signal be a narrowband LFM signal, denoted as

$$s_t(\hat{t}, t_m) = A\mathrm{rect}\left(\frac{\hat{t}}{T_p}\right)\exp\left[j2\pi\left(f_c t + \frac{\mu}{2}\hat{t}^2\right)\right], \tag{1}$$

where $\mathrm{rect}(\cdot)$ is the rectangular window function; $\exp(\cdot)$ is the exponential function; A is the signal amplitude; T_p is pulse width; j is the imaginary unit; f_c is the carrier frequency; μ is the LFM slope; $\hat{t}$ is the fast time; t_m is the slow time, $t_m = mT_r$ (m denotes the mth echo and T_r is the pulse repetition period); t is the total time, $t = \hat{t} + t_m$.

The echo of the rotor after pulse compression and clutter suppression can be expressed as

$$s_r(\hat{t}, t_m) = \sum_{k=1}^{K}\sum_{i=1}^{I}\sigma_{ik}AT_p \sin c\left[B\left(\hat{t} - \frac{2R_{ik}(t_m)}{c}\right)\right] \cdot \exp\left[-j\frac{4\pi}{\lambda}R_{ik}(t_m)\right], \tag{2}$$

where K is the number of blades; I is the number of scattering points on a single blade of the target; σ_{ik} is the scattering coefficient; B is the signal bandwidth; λ is the radar wavelength; $\sin c(\cdot)$ is the distance term, which contains the position information and migration information of the target; $\exp(\cdot)$ is the Doppler term, which contains the Doppler information of the target; $R_{ik}(t_m)$ is the distance from the scattering point on the rotor to the radar.

From the position relationship in Figure 1, the distance from the scattering point on the target to the radar can be written as

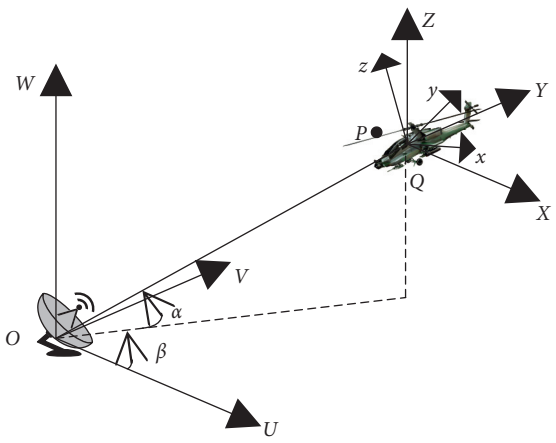

Figure 1: Radar-target position relationship.

$$R_{ik}(t_m) = \left\| \mathbf{R}_0 + \mathbf{v}t + \mathbf{R}_{\mathbf{init}}\mathbf{r}_0 \right\|, \tag{3}$$

where $\mathbf{R}_0$ is the initial distance between the radar coordinate system and the reference coordinate system; $\mathbf{v}$ is the target translational velocity; $\mathbf{r}_0$ is the position of the target scattering point in the target coordinate system, $\mathbf{r}_0 = [r_{ik}\cos(\Omega), r_{ik}\sin(\Omega), 0]^T$, where $\Omega = \omega t_m + \theta_{ik}$, ω is the angular velocity of rotation, θ_{ik} is the initial phase, r_{ik} is the distance of the scattering point from the center of the rotor in the target coordinate system, and $0 \le r_{ik} \le l$; $\mathbf{R}_{\mathbf{init}}$ is the initial rotation matrix determined by the initial Euler angles.

$$\mathbf{R}_{\mathbf{init}} = \begin{bmatrix} a_{11} & a_{12} & a_{13} \\ a_{21} & a_{22} & a_{23} \\ a_{31} & a_{32} & a_{33} \end{bmatrix}. \tag{4}$$

Among them,

$$\begin{cases} a_{11} = \cos\phi_e \cos\varphi_e - \sin\phi_e \cos\theta_e \sin\varphi_e, \\ a_{12} = -\cos\phi_e \sin\varphi_e - \sin\phi_e \cos\theta_e \cos\varphi_e, \\ a_{13} = \sin\phi_e \sin\theta_e, \\ a_{21} = \sin\phi_e \cos\varphi_e + \cos\phi_e \cos\theta_e \sin\varphi_e, \\ a_{22} = -\sin\phi_e \sin\varphi_e + \cos\phi_e \cos\theta_e \cos\varphi_e, \\ a_{23} = -\cos\phi_e \sin\theta_e, \\ a_{31} = \sin\theta_e \sin\phi_e, \\ a_{32} = \sin\phi_e \cos\varphi_e, \\ a_{33} = \cos\theta_e, \end{cases} \tag{5}$$

where ϕ_e is the cross-roll angle; θ_e is the pitch angle; φ_e is the yaw angle. According to the $z-x-z$ regulation [21], the target coordinate system $Q-xyz$ can be transformed into the reference coordinate system $Q-XYZ$ by rotating ϕ_e around the z-axis, θ_e around the x-axis, and φ_e around the z-axis. Then, the coordinate of the scattering point in the reference coordinate system is

$$\mathbf{R}_{\mathbf{init}}\mathbf{r}_0 = \begin{bmatrix} a_{11}r_{ik}\cos\Omega + a_{12}r_{ik}\sin\Omega \\ a_{21}r_{ik}\cos\Omega + a_{22}r_{ik}\sin\Omega \\ a_{31}r_{ik}\cos\Omega + a_{32}r_{ik}\sin\Omega \end{bmatrix}. \tag{6}$$

At this point, the instantaneous frequency of the target echo is

$$f_d = \frac{1}{2\pi}\frac{\mathrm{d}\Phi(t_m)}{\mathrm{d}t_m} = \frac{2}{\lambda}\left[\mathbf{v} + \frac{\mathrm{d}}{\mathrm{d}t_m}\left(\mathbf{R}_{\mathbf{init}}\mathbf{r}_0\right)\right]^{\mathrm{T}}\mathbf{n}. \tag{7}$$

When the target is in the far-field condition, namely, $\|\mathbf{R}_0\| \gg \|\mathbf{v}t_m + \mathbf{R}_{\mathbf{init}}\mathbf{r}_0\|$, $\mathbf{n}$ can be approximated as $\mathbf{n} = \mathbf{R}_0/\|\mathbf{R}_0\|$, which is the line of sight (LOS) direction of the radar. The first term in (7) is the Doppler frequency caused by target translation $f_d = 2\mathbf{v}^{\mathrm{T}}\mathbf{n}/\lambda$, and the second term is the micro-Doppler frequency caused by rotation. Substituting (6). we can obtain

$$f_{m\,D} = \frac{2\omega r_{ik}}{\lambda}\sqrt{m^2+n^2}\sin\left(\Omega - \arctan\frac{n}{m}\right), \tag{8}$$

where $m = a_{11}\cos\alpha + a_{31}\sin\alpha, n = a_{12}\cos\alpha + a_{32}\sin\alpha$. It can be concluded that the echo of the rotor conforms to sinusoidal modulation law and is distributed on both sides centered on the translational Doppler shift. The sideband width is related to the target size, rotation speed, pitch angle, and target attitude. Propeller and jet aircraft are modeled in a similar way and are no longer described here.

3. Classification of Targets

In the classification stage, feature extraction and analysis are first performed on the echoes of three types of targets to find the features with greater differentiation between them. On this basis, suitable feature combinations and classifiers are selected to achieve the classification of different aircraft targets.

3.1. Characteristics Analysis

3.1.1. Flicker Interval. The high-speed rotating parts, such as the main rotor and tail of the helicopter, the propellers of the propeller aircraft, and the turbines of the jet aircraft, on the aircraft target will produce periodic modulation in the radar echo. The periodic modulation caused by such rotating parts was firstly proposed by Professor Chen of the US Naval Laboratory in 2000, who referred to the mechanical vibration and rotation of targets or target components other than center-of-mass advection as micromotion and also named the Doppler modulation phenomenon caused by micromotion in radar echo as the micro-Doppler effect [21–23]. The micro-Doppler effect can reflect the geometric composition and motion characteristics of target structural components, which is a unique feature of the target and can be used to determine the nature of the target, providing a new way for radar target classification. Therefore, using the micro-Doppler characteristics of targets to conduct classification and identification is a current research hotspot.

The fluctuation characteristics of the radar echo vary for different targets. When the rotating part on the target rotates perpendicular to the radar LOS direction, the echo intensity will reach the maximum. When it deviates from the radar LOS direction, the echo intensity will decrease sharply. This phenomenon is known as the time-domain modulation of micromotion, which is called the flicker phenomenon [24]. Figure 2 shows the time-domain echo of three types of

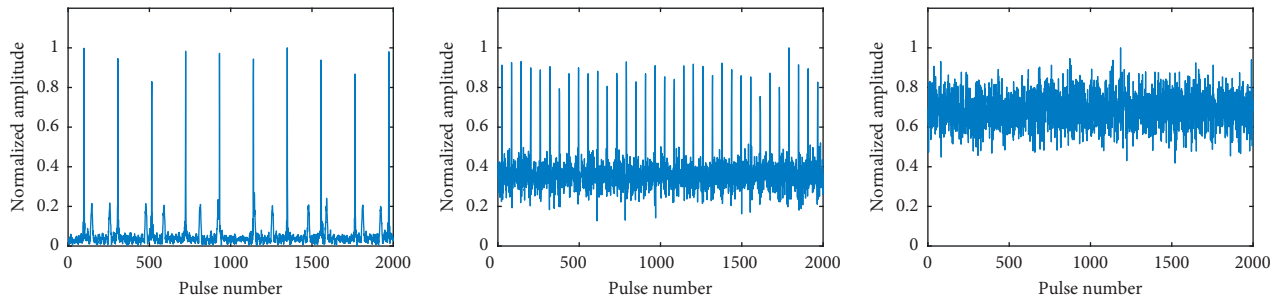

Figure 2: Target echo: (a) helicopter; (b) propeller; (c) jet.

target. The echo of helicopter and propeller aircraft made an obvious flicker phenomenon. Multiple flickers can be observed in a short dwell time, and the flicker interval in the helicopter echo is significantly much longer than that of propeller aircraft. Meanwhile, the flicker in the echo of jet aircraft cannot be detected due to its many blades, small size, and fast rotation speed, and being often obscured. Therefore, the differences of echo amplitude fluctuation of three types of target can be measured by extracting flicker interval.

If the flicker interval is extracted directly in the time-domain echo, it is easily affected by the noise and leads to large error. In order to reduce the adverse impact of noise, this paper improves the extraction accuracy of the target flicker interval by autocorrelation processing, which can improve the output SNR and the estimation accuracy of the flicker interval because there is a correlation between signals, while there is no correlation between signals and noise and noise and noise.

Assuming that the noisy signal is $X(t) = s(t) + n(t)$, the temporal autocorrelation function of its sample function is usually expressed by taking the limit of integration. But under nonideal noise conditions, where the noise is not standard Gaussian white noise, apart from signal autocorrelation and noise autocorrelation, the mutual correlation between signal and noise should be taken into consideration. Thus, the autocorrelation function can be expressed as

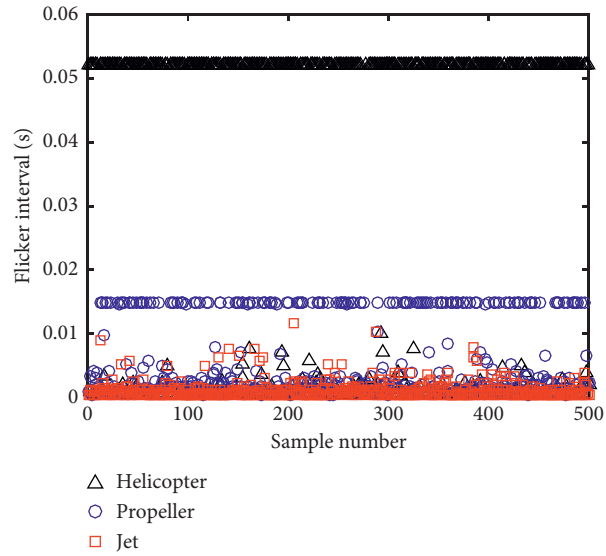

Figure 3: Distribution of flicker interval.

$$R(\tau) = \frac{1}{T}\left(\sum_{i=1,\tau=iT_r}^{T} s(t)s^*(t-\tau) + n^2(t) + \sum_{i=1,\tau=iT_r}^{T} s(t)n^*(t-\tau) + \sum_{i=1,\tau=iT_r}^{T} n(t)s^*(t-\tau)\right), \tag{9}$$

where $(\cdot)^*$ is the conjugate operation. From (9), it can be concluded that, after the autocorrelation process, its SNR is improved by T times. At this point, the flicker interval $\Delta\hat{t}$ can be estimated by finding the peak and subpeak of the autocorrelation function.

$$\Delta\hat{t} = |\tau_1 - \tau_2|, \tag{10}$$

where τ_1 is the delay value when $R(\tau)$ takes the peak and τ_2 is the delay value when $R(\tau)$ takes the subpeak.

The distribution of the time-domain flicker interval extracted by the autocorrelation method is shown in Figure 3, which shows that the flicker interval in the target echo of the rotor helicopter is the largest, while the jet aircraft is the smallest, and the propeller aircraft is between the two. On the premise of accurate flicker interval extraction, the feature can be used to effectively distinguish these three types of targets, but in the actual processing, the flicker interval extraction is not accurate for certain special scenes, so other effective features need to be found to supplement them.

3.1.2. Fractal Dimension. Fractal, an important branch of nonlinear science in recent years, was first introduced into the field of natural science to characterize complex graphs or complex processes. Mandelbrot defined a shape whose components are similar to the whole in some way as a fractal

[25], and the parameter used to characterize the fractal is called the fractal dimension. In 1983, Wheeler pointed out that the importance of fractal to future science is equivalent to the importance of entropy to modern science [26]. Both entropy and fractal are measures of complexity [27–30], but entropy is always dependent on the measurement scale when used to measure multiscale complexity [31, 32], and if the linear scale of measurement is changed, the entropy value changes, which leads to uncertainty, whereas fractal dimension is independent of the measurement scale.

There are many fractal phenomena in nature, such as coastlines, mountain shapes, cloud masses, and grasses. And it has been shown that meteorological clutter, sea clutter, and ground clutter also have fractal properties, so fractal is widely used in the field of radar target detection because the difference of fractal dimension between targets and clutter are obvious, such as target detection in clutter background based on fractal dimension [33]. At the same time, the fractal is considered to have potential in the field of recognition, such as target geometric shape description [34], musical instrument signal classification and recognition [35], and aircraft target classification and identification [36].

Since narrowband radar aircraft targets are mostly under the above three kinds of clutter, the fractal dimension of the same target is relatively stable, and different targets have different fractal dimension due to different geometric shape and modulation characteristic, which makes it possible to classify and identify aircraft targets based on the fractal. The study shows that the fractal dimension is basically unaffected by noise [37], which is practically significant for radar target identification.

Currently, the methods for calculating fractal dimension mainly include the Higuchi method [38] and the box-counting method [19]. Since conducting aircraft target identification requires high real-time performance, this paper uses the box-counting method to calculate the fractal dimension, which is considered to be the fastest and most practical method to calculate the fractal dimension.

Let D be any nonempty bounded subset on $\mathbf{R}^n$ and $N(\varepsilon)$ be the minimum number of sets with a maximum diameter of ε which can cover D. Then, the box dimensions of the upper and lower bounds of D are defined as

$$\begin{cases} \underline{\dim}\, D = \underline{\lim}\limits_{\varepsilon \longrightarrow 0} \dfrac{\log N(\varepsilon)}{-\log \varepsilon}, \\ \overline{\dim} D = \overline{\dim}\limits_{\varepsilon \longrightarrow 0} \dfrac{\log N(\varepsilon)}{-\log \varepsilon}, \end{cases} \tag{11}$$

where $\underline{\dim}$ and $\overline{\dim}$ represent the lower and upper bounds of the box dimension of the set, respectively. If the values of the upper and lower bounds are equal, it is called the box dimension of D and denoted as

$$F\ D = \lim_{\varepsilon \longrightarrow 0} \frac{\log N(\varepsilon)}{-\log \varepsilon}. \tag{12}$$

In the actual calculation, $N_\varepsilon(D)$ is generally taken as an integer multiple of two. If the number of range bins containing the target is N, let

$$\text{cell max} = 2^n > N, \tag{13}$$

where cellmax is the closest power function to N. In (13),

$$\begin{cases} \varepsilon = 2^{(1-e)},\ 1 \le e \le \log_2(\text{cellmax} + 1), \\ N(\varepsilon) = \text{cellmax}/\varepsilon. \end{cases} \tag{14}$$

The box-counting algorithm can be understood as follows: take boxes with side lengths of ε and cover the fractal. Some of the boxes will be empty due to the existence of gaps inside the fractal and then record the number of nonempty boxes as $N(\varepsilon)$. Reduce the size of the boxes and $N(\varepsilon)$ will become larger. According to the definition, the slope of the $\log \varepsilon$ and $\log N(\varepsilon)$ curve in the double logarithmic coordinate system is the fractal dimension. Figure 4 shows the distribution of fractal dimension for the three types of aircraft targets. It can be seen that the fractal dimension of helicopter is the smallest, ranging from 1.4 to 1.5, that of jet aircraft is the largest, ranging from 1.63 to 1.7, and propeller aircraft is between the two, ranging from 1.54 to 1.72. The feature is able to better distinguish helicopter from each other, but the overlap between the feature distribution of jet and propeller aircraft results in a weak differentiation ability of the two targets.

3.1.3. Modulation Bandwidth. In the time-domain echo, the flicker interval is one of the most intuitive indexes that are not easily affected by other factors, and the fractal dimension can be independent of the measurement scale. However, in order to fully characterize the differences in the micromotion characteristics of three types of target, the echo spectrum is also investigated in this paper.

From (8), it can be seen that the frequency modulation caused by the rotation of each scattering point on the target shows a sinusoidal pattern, and the amplitude is determined by the target size, rotation speed, pitch angle, and target attitude. At a certain moment, for the same target, the rotation speed, pitch angle, and target attitude are the same, so the modulation amplitude is only determined by the position of the corresponding scattering point on the rotor. The modulation amplitude caused by the scattering point located at the center of rotation is zero, while the modulation amplitude caused by the scattering point located at the tip of the blade will obtain the maximum value. At this time, the modulation bandwidth of the target is

$$B_{m\,D} = \frac{2\omega l}{\lambda}\sqrt{m^2 + n^2}. \tag{15}$$

In order to obtain the modulation bandwidth of the target, it is necessary to transform the echo from time domain to frequency domain by Fourier transform, and this process can achieve a coherent accumulation effect and has good antinoise performance. Figure 5 shows the spectrum of three types of target echo, where rotor helicopter and propeller aircraft have obvious frequency modulation, and the bandwidth of helicopter is larger than that of propeller aircraft, while the frequency modulation phenomenon

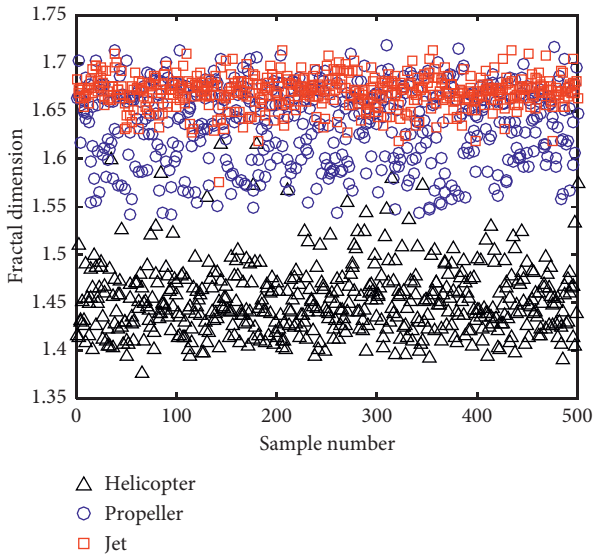

Figure 4: Distribution of fractal dimension.

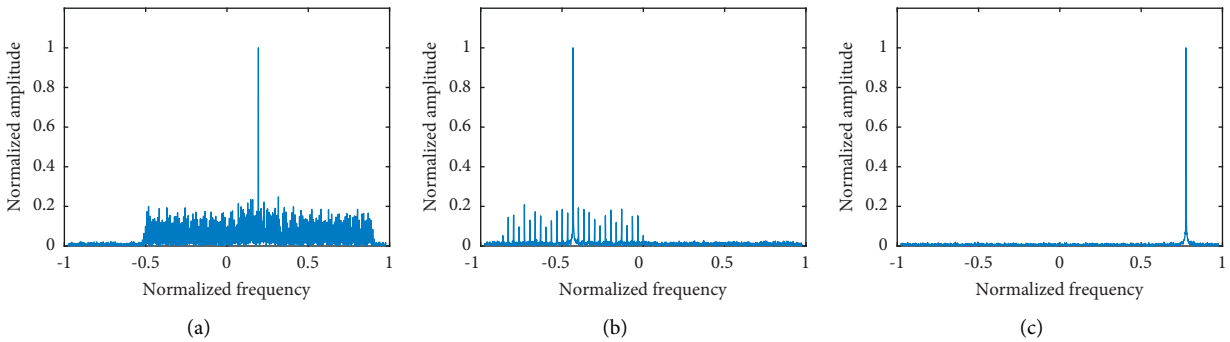

Figure 5: Frequency spectrum: (a) helicopter; (b) propeller; (c) jet.

caused by micromotion cannot be detected in the echo of jet aircraft. Therefore, the differences in frequency spectrum can be measured by extracting the frequency modulation bandwidth.

In this paper, the modulation bandwidth is calculated by taking the envelope of the spectrum, using the mean value of the envelope amplitude as the threshold, and setting the envelope values smaller than the threshold to zero. Its distribution is shown in Figure 6. From the distribution of the modulation bandwidth, it can be seen that the bandwidth of the jet aircraft target is small, only 200 Hz, and its distribution range is very concentrated, which is because of the fact that there is no micro-Doppler effect in this type of target echo; that is, micro-Doppler modulation does not occur. In contrast, the modulation bandwidth distribution of rotor helicopter and propeller aircraft is more complex, and it can be seen in Figure 5 that the rotor helicopter target echo bandwidth is slightly larger than that of propeller aircraft, but after taking the target attitude and feature extraction method into consideration, the rotor helicopter echo modulation bandwidth is mainly concentrated in 1800–2800 Hz, and the propeller aircraft echo modulation bandwidth is distributed in 500–2800 Hz. Therefore, this feature is able to distinguish jet aircraft better, while it does weakly in distinguishing rotor helicopter and propeller aircraft.

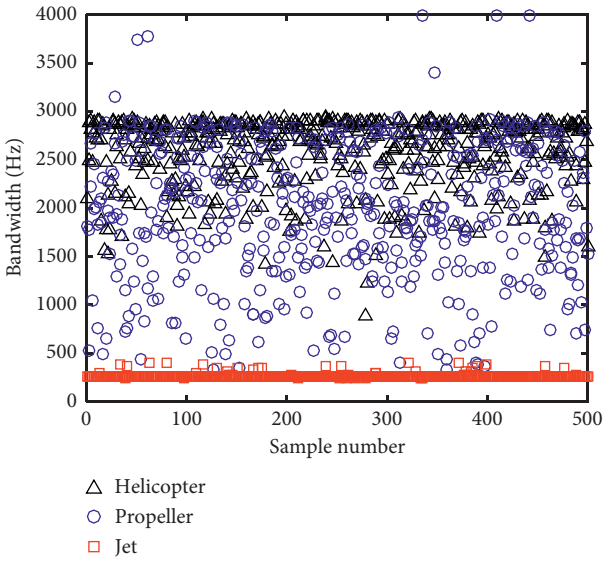

Figure 6: Distribution of modulation bandwidth.

3.1.4. Second Central Moment. Although the modulation bandwidth can measure the differences of three types of target in the frequency domain to a certain extent and enjoys some noise immunity, there are some errors under the influence of attitude and feature extraction method, and the robustness of the feature is insufficient. Therefore, this paper also extracts the classical feature of the second central moment in frequency domain to realize the classification. For a signal spectrum sequence $X = \{X_i\}_{i=1}^{N}$, its second central moment is

$$U^2 = \sum_{i=1}^{N} (i - i_0)^2 \overline{X_i}, \tag{16}$$

where $\overline{X_i} = X_i / \sum_{i=1}^{N} X_i$ and $i_0 = \sum_{i=1}^{N} i \cdot \overline{X_i}$. The second central moment characteristic in the frequency domain reflects the sparsity of the deviation of the frequency-domain echo relative to its geometric center of gravity. According to Figure 5, it can be seen that, for helicopter, the geometric center of gravity of the spectrum is mainly determined by the fuselage component, and the other components are concentrated near the fuselage component; that is, the deviation relative to the geometric center of gravity is dense and the second central moment is the smallest, while jet aircraft is just the opposite, which enjoys the largest second central moment, and propeller aircraft is in between. Its distribution is shown in Figure 7.

In practical systems, information such as target RCS and actual velocity can also be obtained, which can be used to further improve the classification performance, but these features are not used in this paper due to the limitation of a priori information and real-time requirements.

4. Classification Method

The flicker interval, fractal dimension, modulation bandwidth, and second central moment are used to classify three types of target, and the processing steps are as follows:

(1) Simulated echo generation: aimulated radar echoes are generated by using the scattering point model and processed for pulse compression and clutter suppression to obtain a range-azimuth amplitude map. The range bin where the target is located is determined from the target detection results, and the slow time dimensional data within that range bin is extracted.

(2) Feature combination acquisition: the fractal dimension is extracted from the slow time dimensional data using a box-counting algorithm, and the flicker interval is extracted by autocorrelation in time domain. Subsequently, the Fourier transform is then used to transform the slow time dimensional data into the frequency domain to calculate the second central moment, the modulation bandwidth is extracted using the idea of taking the envelope over the threshold, and these four feature values are used as feature combination for the classification of three types of target.

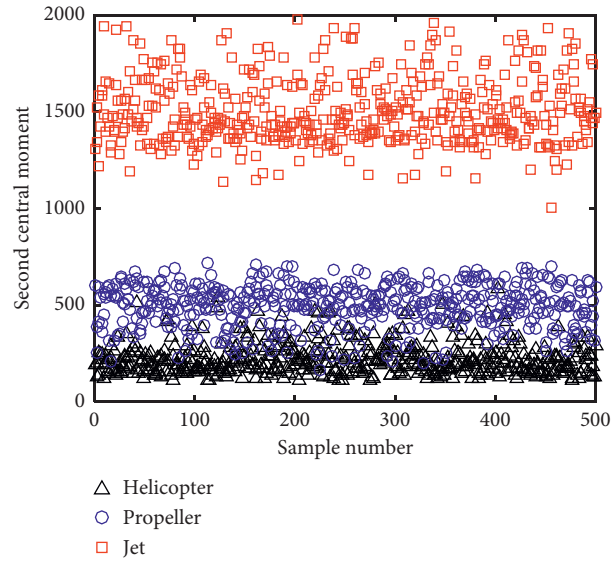

Figure 7: Distribution of second central moment.

(3) Classifier design: the extracted feature combination is fed into three binary SVM classifiers for classification. The first classifier is used to distinguish between rotor helicopter and propeller aircraft, the second classifier is used to distinguish between rotor helicopter and jet aircraft, the third classifier is used to distinguish between propeller aircraft and jet aircraft, and the final classification results are obtained by a voting mechanism. The classifier model is shown in Figure 8.

In Figure 8, both training and test data are generated for simulation, with a total of 21 SNR sampling points and 500 sets of data under each sampling point. Among them, 150 sets are randomly selected as the training dataset for each classification, the remaining 350 sets are used as the test dataset, and the average classification accuracy under each SNR sampling point is obtained as the final classification accuracy by 100 Monte-Carlo experiments.

4.1. Simulation Analysis. In order to be closer to reality, the scattering point model used in this paper fully considers the main structure of the target, such as the fuselage, main rotor, tail, and weapon mount. Assume that the backscattering properties of the materials used in the target are basically the same; that is, the scattering points are assumed to be uniformly distributed, and the scattering intensity is the same. The scattering point models of three types of target are shown in Figure 9, and the specific target parameters are set as Table 1. The difference is ensured by randomly selecting the target's attitude to ensure that the variability of each simulation, the target's cross-roll angle, longitudinal sway angle, and yaw angle in the simulation obey the uniform distribution on $(-\pi/2, \pi/2)$, $(-\pi/6, \pi/6)$, and $(-\pi/12, \pi/12)$, respectively, and the target flight direction is determined by its attitude. The radar parameters are referenced to a conventional narrowband air surveillance radar with a carrier

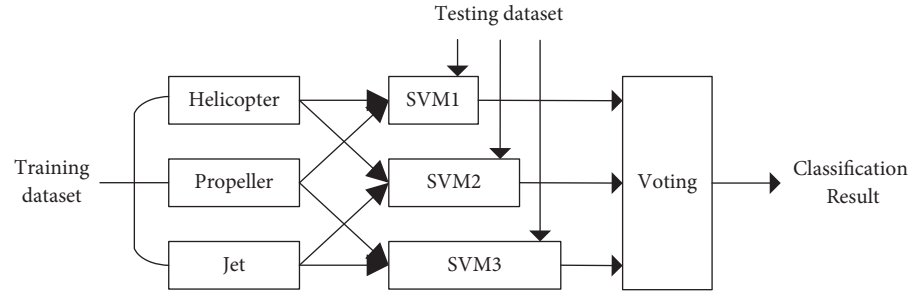

Figure 8: Three-class SVM model.

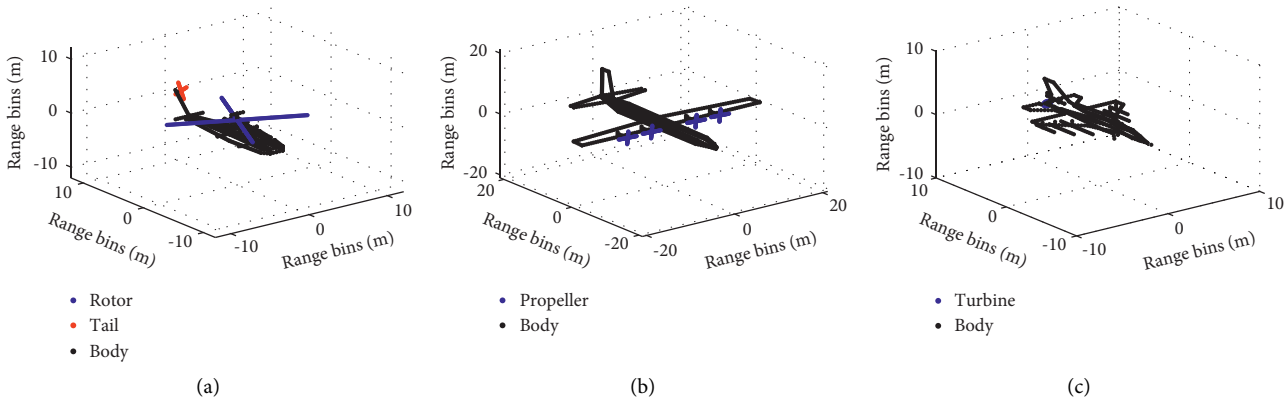

Figure 9: Scattering point model: (a) helicopter; (b) propeller; (c) jet.

Table 1: Target parameters.

Parameters	Helicopter	Propeller	Jet
Number of rotors	2	4	1
Number of blades	3/4	4	21
Length (m)	7.3/1.4	2.05	0.44
Rotation speed (r/min)	288/360	1020	5000
Distance (m)	28000	28000	28000
Height (m)	1500	5000	7000
Speed (m/s)	81	150	289

frequency of 1 GHz, bandwidth of 2 MHz, and pulse repetition frequency of 4000 Hz. It should be pointed out that all the SNR mentioned are the SNR after pulse compression.

The target can be detected, and its azimuthal dimensional data can be obtained by clutter suppression of the target echo. The flicker interval, fractal dimension, modulation bandwidth, and second central moment features in frequency domain are extracted and classified by a three-classification SVM classifier. After 100 Monte-Carlo experiments, the average classification probability of the three types of target under different SNR conditions is shown in Figure 10. It is worth pointing out that the SNR after pulse compression of conventional narrowband surveillance radar is usually above 5 dB, and the target may not be detected when the SNR is low, so the SNR region is set from −10 dB to 10 dB in this paper.

From the classification results, it can be concluded that the classification of targets based on the method proposed in this paper has the highest classification probability of 100%

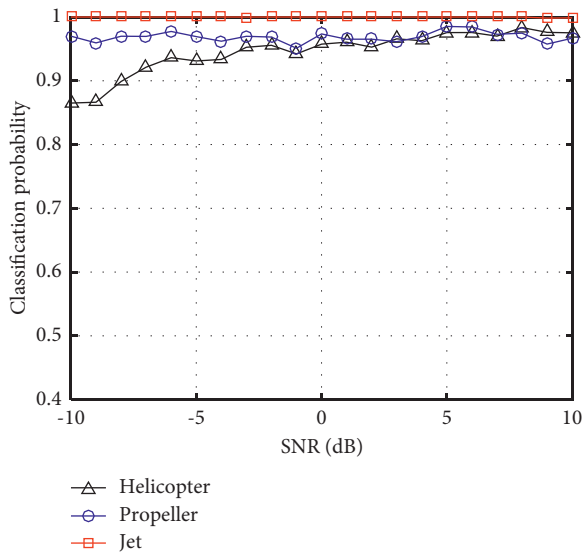

Figure 10: Classification result.

for jet aircraft because the feature distribution of jet aircraft is relatively simple in the feature combination proposed in this paper, and its feature distribution basically does not overlap with the rotor helicopter and propeller aircraft. Similarly, it is due to the more overlapping feature distribution of rotor helicopter and propeller aircraft that the classification probability of these two types of targets is comparatively low, with the best classification probabilities of 98.49% and 98.31%, respectively. As the SNR decreases,

the classification probability of jet aircraft remains essentially unchanged, and that of propeller aircraft changes relatively flat, but that of rotor helicopter is more variable, with a classification probability of only 86.37% at SNR = −10 dB.

In order to verify the advances of the proposed method in this paper, the proposed method is also compared with the methods used in [17] (method 1), [18] (method 2), [19] (method 3), and [20] (method 4) for the target classification performance, and the comparative simulation result is shown in Figure 11.

From Figure 11, it can be seen that the average classification probability of the three types of target in the proposed method is the highest and the classification probability is more stable under different SNR conditions, maintaining above 93.72%. The classification probability of the feature combination proposed in method 1 is seriously influenced by noise, and it is more stable at SNR >5 dB and can be maintained at about 87.80%, but the classification probability decreases rapidly as the SNR decreases, and the classification probability is only 47.12% when SNR = −10 dB. In comparison, the classification performance of method 2 is the best among the four compared methods, with a classification probability of 93.65% at high SNR and a classification probability of more than 80% at low SNR, but it is still not comparable to the performance of the proposed method. The classification performance of method 3 and method 4 is close because both methods use amplitude fluctuation feature; besides, the fractal feature used in method 3 and the entropy feature used in method 4 have some similarities. And because the proposed feature combination in these two methods does not use more feature values, which can accurately describe the properties of the target echo, the classification probability is not high, and the best classification probability is only 79.93% and 81.16%. Thus, it can be seen that the proposed feature combination in this paper has good robustness and the classification performance is significantly higher than the existing methods.

Further demonstrations of the reasons for the better classification performance of the proposed method compared with [17–20]. (1) The fundamental reason is that this paper extracts the time-domain flicker interval and frequency-domain modulation bandwidth based on the micro-Doppler modulation characteristics of the target echo, which are more discriminative than the traditional statistical features. Meanwhile, the proposed fractal dimension is not affected by noise, and both the time-domain flicker interval and the frequency-domain modulation bandwidth enjoy strong antinoise ability, but they are not discussed in any existing methods. (2) Compared with [17], which uses a single frequency-domain feature, the combination of features proposed in this paper covers both time-domain features and frequency-domain features, which can more comprehensively characterize the potential information contained in the signal. The feature combination proposed in [17] is obtained by the EMD algorithm, which lacks a complete theoretical basis, and the modal aliasing and endpoint effects in its IMF components will lead to false frequency distributions, which cannot accurately

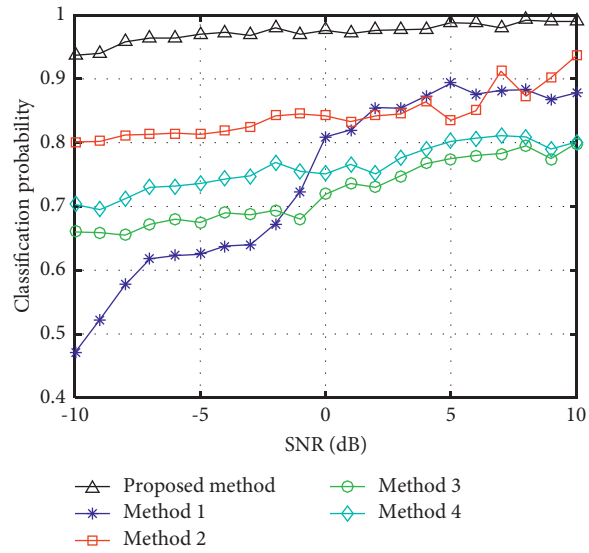

Figure 11: Comparative simulation result.

characterize the frequency-domain properties of the target. Moreover, the proposed modal energy ratio feature is not robust in low SNR or strong clutter environment. (3) Reference [18] obviously proposes multiple features in the time domain, frequency domain, and time-frequency domain to analyze the target echo, which has one more dimension than the method in this paper, but the proposed feature combination is not universal and has poor performance in the data used in this paper. In terms of Doppler shift, this parameter is obviously influenced by the direction of the target flight; for example, a helicopter target can obtain a large Doppler shift when the angle between the helicopter and the radar LOS direction is small; while the angle between the jet and the radar LOS direction is large, its Doppler shift will be small, so the classification stability is poor by using this feature directly. Meanwhile, [18] utilized entropy features in multiple domains, which are susceptible to the measurement scale and the resolution of the time-frequency analysis method in the time-frequency domain and do not have advantages over the fractal feature proposed in this paper. (4) Reference [19] verified the effectiveness of using the fractal feature for target classification using measurement data, but the proposed feature combination is too single, with only two time-domain features. Compared with the multidimensional and multifeature of the proposed method, it has obvious disadvantages. (5) The feature combination proposed in [20] is more adaptable in the case of a small number of scattering points, but the three types of target models used in this paper are composed of a large number of scattering points, so the performance degrades seriously, while the feature combination proposed in this paper is actually less affected by the target model and the performance is more stable.

5. Conclusion

For conventional narrowband radar, the characteristics of Doppler shift, amplitude fluctuation, and time-frequency

spectrum are directly extracted to classify the three types of targets, which are susceptible to unfavorable factors such as noise and computation, and the classification probability is not high. However, the concept of the micro-Doppler effect makes scholars realize that the micromotion information on the target reflects the essential characteristics of the target to a certain extent, which provides a new way for the classification. In this paper, the micro-Doppler modulation is analyzed from time domain and frequency domain, and a novel classification method based on the feature combination of flicker interval, fractal dimension, modulation bandwidth, and second central moment is proposed. Simulation results show that this method is insensitive to noise and has high robustness. Compared with the existing methods, it has a higher classification probability, which can be maintained above 93.72%.

Data Availability

The experimental simulation data used to support the findings of this study are available from the corresponding author upon request.

Conflicts of Interest

The authors declare no conflicts of interest.

Acknowledgments

This work was supported in part by the National Natural Science Foundation of China under Grant 61671469, the Key Project of the Army Equipment Department under Grant KJ20201A020301, and the Foundation Project of Air Force Early Warning Academy under Grant HJGC2021001.

References

[1] J. Liu, N. Fang, Y. Jun Xie, and B. Fa Wang, "Scale-space theory-based multi-scale features for aircraft classification using HRRP," *Electronics Letters*, vol. 52, no. 6, pp. 475–477, 2016.

[2] J. Yuan, Y. Li, J. Cai, Y. Wang, and J. Xu, "Robust automatic target recognition via HRRP sequence based on scatterer matching," *Sensors*, vol. 18, no. 2, 2018.

[3] I. F. Zhao, Y. Liu, K. Huo, S. Zhang, and Z. Zhang, "Radar HRRP target recognition based on stacked autoencoder and extreme learning machine," *Sensors*, vol. 18, no. 1, 2018.

[4] N. Tang, X.-Z. Gao, and X. Li, "Target classification of ISAR images based on feature space optimisation of local non-negative matrix factorisation," *IET Signal Processing*, vol. 6, no. 5, pp. 494–502, 2012.

[5] K. Ayoub, T. Abdelmalek, K. Ali, and E. H. Mohammed, "Radar target recognition using salient keypoint descriptors and multitask sparse representation," *Remote Sensing*, vol. 10, no. 6, 2018.

[6] W. Yunpeng, H. Yihua, L. Wuhu, and G. Liren, "Aircraft target classification method based on texture feature of laser echo Time-Frequency image," *Acta Optica Sinica*, vol. 37, no. 11, Article ID 1128004, 2017.

[7] K. Fu, W. Dai, Y. Zhang, W. Zhirui, Y. Menglong, and S. Xian, "MultiCAM: multiple class activation mapping for aircraft recognition in remote sensing images," *Remote Sensing*, vol. 11, no. 5, 2019.

[8] X. Pan, F. Yang, L. Gao et al., "Building extraction from High-Resolution aerial imagery using a generative adversarial network with spatial and channel attention mechanisms," *Remote Sensing*, vol. 11, no. 8, 2019.

[9] G. Zheng and Y. Song, "Signal model and method for joint angle and range estimation of low-elevation target in meter-wave FDA-MIMO radar," *IEEE Communications Letters*, Article ID 3126935, 2021.

[10] G. Zheng, Y. Song, and C. Chen, "Height measurement with meter wave polarimetric MIMO radar: signal model and MUSIC-like algorithm," *Signal Processing*, vol. 190, Article ID 108344, 2022.

[11] J. Bae and N. A. Goodman, "Widely separated MIMO radar with adaptive waveform for target classification," in *Proceedings of the 2011 4th IEEE International Workshop on Computational Advances in Multi-Sensor Adaptive Processing (CAMSAP)*, pp. 21–24, San Juan, PR, USA, December 2011.

[12] G. J. Melendez and S. B. Kesler, "Spectrum estimation by neural networks and their use for target classification by radar," in *Proceedings Icassp IEEE International Conference on Acoustics Speech & Signal Processing*, vol. 5, pp. 3615–3618, Detroit, MI, USA, May 1995.

[13] F. Chen, H. Liu, L. Du, and Z. Bao, "Target classification with low-resolution radar based on dispersion situations of eigenvalue spectra," *Science China Information Sciences*, vol. 53, no. 7, pp. 1446–1460, 2010.

[14] P. Kang and Z. Chen, "Aircraft classification method based on the kurtosis - skewness feature and wavelet decomposition and linear discriminant analysis," *Journal of Engineering*, vol. 2019, no. 21, pp. 7855–7859, 2019.

[15] J. H. Ma, H. W. Liu, and Z. Bao, "Research on helicopter and fixed-wing aircraft classification," *Modernradar*, vol. 12, pp. 45–48, 2004.

[16] Y. Zhao, Z. Chen, B. Jiu, L. Zhang, and Z. Li, "Narrow-band aircraft targets feature extraction and classification based on time-frequency analysis," *Journal of Electronics and Information Technology*, vol. 39, no. 9, pp. 2225–2231, 2017.

[17] B. S. Wang, L. Du, H. W. Liu, and F. Bo, "Aircraft classification based on empirical mode decomposition," *Journal of Electronics and Information Technology*, vol. 34, no. 9, pp. 2116–2121, 2012.

[18] L. Ming, J. Wu, Z. Lei, and S. Wanjie, "Aircraft target classification and recognition algorithm based on measured data," *Journal of Electronics and Information Technology*, vol. 40, no. 11, pp. 2606–2613, 2018.

[19] F. Y. Wang, L. Ding, and H. W. Liu, "Low-resolution airborne radar aircraft target classification," *Journal of Radars*, vol. 3, no. 4, pp. 444–449, 2014.

[20] W. Wang, Z. Tang, Y. Chen, Z. Yuanpeng, and S. Yongjian, "Aircraft target classification for conventional narrow-band radar with multi-wave gates sparse echo data," *Remote Sensing*, vol. 11, no. 22, 2019.

[21] V. C. Chen, D. Tahmoush, and W. J. Miceli, *Radar Micro-Doppler Signatures: Processing and Applications*, IET Digital Library, London, UK, 2014.

[22] V. C. Chen, F. Fayin Li, S. S. Shen-Shyang Ho, and H. Wechsler, "Micro-Doppler effect in radar: phenomenon, model, and simulation study," *IEEE Transactions on Aerospace and Electronic Systems*, vol. 42, no. 1, pp. 2–21, 2006.

[23] V. C. Chen, F. Li, S.-S. Ho, and H. Wechsler, "Analysis of micro-Doppler signatures," *IEE Proceedings - Radar, Sonar and Navigation*, vol. 150, no. 4, pp. 271–276, 2003.

[24] Y. B. Chen, D. Li Sha, J. Yang, and R. Cao Fu, "Rotor blades radar echo modeling and its mechanism analysis," *Acta Physica Sinica*, vol. 16, no. 13, Article ID 138401, 2016.
[25] X. Chen, J. Guan, Y. He, and J. Zhang, "Detection of low observable moving target in sea clutter via fractal characteristics in fractional fourier transform domain," *IET Radar, Sonar & Navigation*, vol. 7, no. 6, pp. 635–651, 2013.
[26] J. A. Wheeler, "Review on the fractal geometry of nature by benoit B. Mandelbrot," *American Journal of Physics*, vol. 51, no. 4, pp. 286-287, 1983.
[27] P. Bak, *How Nature Works: The Science of Self-Organized Criticality*, Springer, Manhattan, NY, USA, 1996.
[28] F. Cramer, *Chaos and Order: The Complex Structure of Living Systems*, VCH Publishers, Hoboken, NJ, USA., 1993.
[29] S. M. Pincus, "Approximate entropy as a measure of system complexity," *Pnas*, vol. 88, no. 6, pp. 2297–2301, 1991.
[30] Y. Chen, "Equivalent relation between normalized spatial entropy and fractal dimension," *Physica A: Statistical Mechanics and its Applications*, vol. 553, Article ID 124627, 2016.
[31] Y. Bar-Yam, "Multiscale complexity/entropy," *Advances in Complex Systems*, vol. 7, pp. 47–63, 2004.
[32] Y. Bar-Yam, "Multiscale variety in complex systems," *Complexity*, vol. 9, no. 4, pp. 37–45, 2004.
[33] F. Y. Wang, G. R. Jiang, and H. Ming, "Balloon borne radar target detection within ground clutter based on fractal character," National Defense Invention Patent, Patent ID No.201110015890.X, 2011.
[34] C. Chang and S. Chatterjee, "Fractal based approach to shape description, reconstruction and classification," in *Proceedings of the Twenty-Third Asilomar Conference on Signals, Systems and Computers*, Pacific Grove, CA,USA, October 1989.
[35] A. Zlatintsi and P. Maragos, "Multiscale fractal analysis of musical instrument signals with application to recognition," *IEEE Transactions on Audio Speech and Language Processing*, vol. 21, no. 4, pp. 737–748, 2013.
[36] A. K. Mishra, H. Feng, and B. Mulgrew, "Fractal feature based radar signal classification," in *Proceedings of the IET International Conference on Radar Systems*, Edinburgh, UK, October 2007.
[37] M. Salmasi and M. Modarres-Hashemi, "Design and analysis of fractal detector for high resolution radars," *Chaos, Solitons & Fractals*, vol. 40, no. 5, pp. 2133–2145, 2009.
[38] B. S. Raghavendra and D. N. Dutt, "Signal characterization using fractal dimension," in *Proceedings of the TENCON 2008 - 2008 IEEE Region 10 Conference*, vol. 18, no. 3, pp. 287–292, Hyderabad, India, November 2008.